




# Forcing mechanisms of orbital-scale changes in winter rainfall over northwestern China during the Holocene

The Holocene  
1–7  
© The Author(s) 2015  
Reprints and permissions:  
sagepub.co.uk/journalsPermissions.nav  
DOI: 10.1177/0959683615612569  
hol.sagepub.com  


Xiaojian Zhang, Liya Jin, Wei Huang and Fahu Chen

## Abstract

The moisture history in arid central Asia (ACA) differs from that in the Asian monsoon region during the Holocene. Much less is known about causes of Holocene moisture changes in ACA than Asian monsoon precipitation changes, hampering our understanding of their spatiotemporal differences. In this study, orbital-scale evolution of winter rainfall in northwestern China (a part of the core zone in ACA) during the Holocene and possible driving mechanisms are investigated using results from a long-term transient simulation performed by an atmosphere–ocean–sea-ice coupled general circulation model, the Kiel Climate Model, forced by orbital variations. Our results reveal a persistent wetting trend in northwestern China in winter throughout the Holocene, which is in response to winter insolation at mid-northern latitudes. Winter insolation can influence the rainfall via three ways. First, increasing latitudinal gradient of the incoming solar insolation at mid-latitudes strengthens the westerly intensity. Second, the evaporation is enhanced because of insolation-induced winter temperature rising, resulting in an increase in the air humidity. Intensified westerly winds and the increased water vapour together are conducive to enhance moisture transport towards northwestern China and thus increase winter precipitation in this area. Third, the increasing trend of winter insolation weakens the East Asian winter monsoon, which is favourable for the formation of rainfall via crippling the Siberian High that is beneficial for atmospheric lifting motion.

## Keywords

arid central Asia, Holocene, insolation, paleoclimate simulation, precipitation, westerly winds

Received 28 June 2015; revised manuscript accepted 2 September 2015

## Introduction

The mid-latitude Asian continent comprises two distinct climatic regions (Chen et al., 2008, 2010; Dando, 2005): monsoon circulation-dominated humid eastern part of Asia and mid-latitude westerlies-controlled arid central Asia (ACA). ACA is one of the largest arid (desert) areas in the world, including several central Asian countries, northwestern China, and southern Mongolian Plateau. In the past decades, under the context of greenhouse gas (GHG)-induced global warming, the East Asian summer monsoon (EASM) intensity in northern China experienced a persistent weakening trend (e.g. Ding et al., 2008, 2009; Ye and Lu, 2012), whereas climate in northwestern China has shifted from dry to wet (Chen et al., 2011; Feng et al., 2007; Huang et al., 2015a; Jiang et al., 2005; Shi et al., 2007; Su and Wang, 2007; Xu et al., 2015). On interannual to decadal time scales, the Northern Hemisphere circumglobal teleconnection (CGT) was suggested to be a key factor affecting the leading mode of summer rainfall variations in northwestern China (Chen and Huang, 2012; Huang et al., 2011, 2015a, 2015b). The CGT pattern is triggered and maintained by the diabatic heating of Indian summer monsoon (ISM) precipitation (Chen and Huang, 2012; Ding and Wang, 2005; Yang et al., 2007). During weak ISM years, the negative phase of the CGT can induce anomalous moisture transport from the Indian Ocean towards northwestern China, to potentially increase summer precipitation in northwestern China (Huang et al., 2015b). In contrast, the negative phase of the CGT tends to reduce precipitation in the EASM region because of weakened

moisture transport from the western Pacific Ocean (Ding and Wang, 2005). As such, the CGT pattern may have played an important role in the inverse relationship between summer precipitation in northwestern China and the EASM region (Huang et al., 2015a). The CGT tends to be weakened under anthropogenic global warming because of atmospheric stabilization and decreasing relationship with ISM as well as weakening of the ISM–El Niño–Southern Oscillation relationship (Lee et al., 2014), which can further intensify precipitation in northwestern China and reduce precipitation in the EASM region. In winter, precipitation in northwestern China is related to weak North Atlantic Oscillation or Arctic Oscillation (NAO or AO) (Aizen et al., 2001; Huang et al., 2013) and strong mid-latitude westerly winds (Huang et al., 2013), both of which can increase moisture transport from the North Atlantic to northwestern China and hence enhanced precipitation in this region.

Key Laboratory of Western China's Environmental Systems, Ministry of Education, College of Earth and Environmental Sciences, Lanzhou University, China

## Corresponding author:

Liya Jin, Key Laboratory of Western China's Environmental Systems, Ministry of Education, College of Earth and Environmental Sciences, Lanzhou University, Lanzhou 730000, China.  
Email: jinly@lzu.edu.cn

**Table 1.** KCM Holocene simulation conditions and input.

	Eccentricity	Obliquity	Precession	CO <sub>2</sub> (ppm)	CH <sub>4</sub> (ppb)	N <sub>2</sub> O (ppb)
H0K	0.0167	23.4°	102°	286.2	805.6	276.7
H9K	0.0194	24.2°	303°	Same as H0K		
HT	Varying from H9K to H0K			Same as H0K		

KCM: Kiel Climate Model; HT: Holocene transient.

The spatiotemporal features of climate and environment changes during the Holocene in the mid-latitude Asian continent have attracted great attention. Chen et al. (2008) revealed an out-of-phase relationship in moisture evolution during the Holocene between the ACA (synthesized from 11 lake records) and EASM regions, showing that ACA experienced a dry early Holocene, a wetter early to mid-Holocene, and a moderately wet late Holocene, which was in contrast to the EASM evolution throughout the Holocene. It is found that the out-of-phase relationship between moisture changes in ACA and monsoon-dominated Asia existed on the orbital scale not only during the Holocene (An et al., 2012; Chen et al., 2008; Huang et al., 2009; Long et al., 2014) but also during last millennial scale (Chen et al., 2006, 2010, 2015). In the study of Chen et al. (2008), however, the region of ACA is divided apart from the EASM region based on modern Asian summer monsoon limit, which raises a question that some proxy records influenced by the EASM during the early to middle Holocene were categorized into ACA, causing erroneous estimation of the moisture evolution in ACA. This is due to the fact that the intertropical convergence zone (ITCZ) shifted much more northward during the early to middle Holocene compared with the present (Haug et al., 2001), leading to a northward migration of the Asian summer monsoon limit. Recent study found that the core region influenced by the westerlies includes Xinjiang in China during the instrumental period (Huang et al., 2015a). Wang and Feng (2013) synthesized four records from northern Xinjiang, showing a wetting trend in northern Xinjiang over the past 8000 years and an inverse relationship with the EASM. An aeolian sedimentary sequence from Bayanbulak Basin in Tianshan Mountains also indicated relatively wetter climate existed during the middle to late Holocene in the core ACA area (Long et al., 2014), which is also supported by the vegetation history in and around the middle Caspian (Leroy et al., 2014).

The weakening EASM during the Holocene is attributed to reducing summer insolation (e.g. Jin et al., 2014; Wang et al., 2005). Driving factors for the climate change in ACA during this period, however, were only sporadically investigated. The increasing trend of winter insolation and associated cold-season temperature in northwestern Europe were suggested to be responsible for the wetting trend of northern Xinjiang during the past 8 ka (Wang and Feng, 2013). This is partially supported by the modelling work from Jin et al. (2012). Jin et al. (2012) indicated that the early Holocene (8.5 ka BP) desertification in ACA was mainly caused by orbital forcing that weakened mid-latitude westerlies and reduced the upstream evaporation in boreal winter. In addition, the presence of the remnant Laurentide ice sheets (LIS) and deglacial freshening of the North Atlantic reduced the water vapour transport from the Mediterranean, Black and Caspian Seas to ACA in winter during the early Holocene, exacerbating the early Holocene desertification in ACA (Jin et al., 2012). Despite the above studies, it is still insufficient to reveal physical mechanisms of moisture changes in ACA throughout the Holocene. In this study, we investigated the behaviour of winter precipitation in northwestern China (a core zone in ACA) and associated driving factors during the Holocene via analysing results from a transient simulation performed by a coupled general atmosphere–ocean–sea-ice model.

## Methods

### Model description

The model used in this study is the Kiel Climate Model (KCM) (Park et al., 2009), a coupled general atmosphere–ocean–sea-ice model. The model comprises the spectral atmospheric model ECHAM5 (Roeckner et al., 2003) and the Nucleus for European Modelling of the Ocean (NEMO) (Madec, 2008) ocean–sea-ice general circulation model, coupled through OASIS3 (Valcke, 2006). Models described here did not couple anomalies or use a flux correction. The horizontal resolution of ECHAM5 is T31 (3.75° × 3.75°), and in the vertical direction there are 19 levels up to 10 hPa. The horizontal resolution of NEMO is on average 1.3° based on 2° Mercator meshes with grid refinement in the tropical regions, where the meridional grid-point separation reaches 0.5°. NEMO assumes 31 vertical levels. The KCM has been used for studies of internal climate variability (Park and Latif, 2008, 2010), external forced variability (Latif et al., 2009) and the Holocene Asian summer monsoon precipitation changes (Jin et al., 2014; Zhang et al., 2015). A detailed description of the KCM is given by Park et al. (2009), including further information on the performance of the model.

### Numerical experiments

We conducted three simulations using the KCM. First, two equilibrium simulations for two time slices were performed using the KCM: the early Holocene (9500 years before present (BP), H9K) and the pre-industrial (AD 1800, H0K), respectively. The experiments H9K and H0K were both initialized with Levitus climatology data (Levitus, 1982) and integrated for 1000 years under the orbital configurations (eccentricity, obliquity and precession; Berger and Loutre, 1991) for 9.5 and 0 ka BP, respectively. GHG (i.e. the atmospheric concentrations of CO<sub>2</sub>, CH<sub>4</sub> and N<sub>2</sub>O) concentrations were held constant at pre-industrial levels.

After the two equilibrium simulation experiments, we performed a Holocene transient (HT) simulation forced by the Earth's orbital forcing for the period from 9.5 to –0.5 ka BP (500 years after present). The HT simulation started from the last year of the equilibrium experiment H9K. The orbital parameters (Berger and Loutre, 1991) were varied from 9.5 to –0.5 ka BP under a 10× acceleration scheme (Lorenz and Lohmann, 2004) to efficiently manage computational resources. As such, the climate trends and feedbacks of the last 9500 years (9.5–0 ka BP) and the next 500 years (0 to –0.5 ka BP), imposed by the external orbitally driven insolation changes, were represented in the experiment by 1000 model years in 10-year intervals. The GHG concentrations were the same as in the control run. Boundary conditions for the three simulations are further summarized in Table 1.

The performance of the KCM in modelling Holocene climate in Asia has been examined by Jin et al. (2014) and Dallmeyer et al. (2015). The KCM reproduces well the general feature of Holocene climate (precipitation and temperature) in northwestern China.

### Definition of westerly intensity index

It is essential to define an index to measure the strength of the mid-latitude westerlies that have been suggested to be a key factor affecting Holocene moisture evolution in ACA (e.g. Wang and Feng, 2013). The strength of the mid-latitude westerlies can

simply be measured by zonal mean winds (westerlies) averaged over a selected area (e.g. 35°–55°N and 0°–90°E in this study). In addition, the westerly geostrophic wind ( $u_g$ ), which is described in detail in the following, is used to indicate the westerly intensity and to reflect the dynamic mechanism of westerly circulation.

Due to the difference in solar heating between mid-latitude and subpolar regions, winds across the mid-latitudes would blow in a poleward direction if the Earth were a non-rotating planet. However, the Coriolis effect caused by the rotation of Earth induces winds to steer to the right (left) in the Northern (Southern) Hemisphere (Figure 1). Therefore, winds across the mid-latitudes tend to blow from the west towards the east, referred to as the prevailing westerlies. The strength of the mid-latitude westerlies then can be estimated using the geostrophic balance (Holton, 2004), in which the Coriolis force ( $f \bullet u_g$ , where  $f$  is the Coriolis parameter) is balanced by the pressure gradient force ( $-\partial\Phi/\partial y$ , where  $\Phi$  is the geopotential height) (Figure 1). Therefore,

$$f \bullet u_g = -\frac{\partial\Phi}{\partial y}$$

We thus obtain

$$u_g = -\frac{1}{f} \bullet \frac{\partial\Phi}{\partial y}$$

The westerly intensity index can be further simplified to the difference in geopotential height between 35°N and 55°N (Rossby et al., 1939). Since geopotential height is closely related to air temperature, this westerly intensity index can dynamically and thermodynamically relate the mid-latitude westerlies to insolation forcing on orbital time scales.

## Evolution of boreal winter rainfall in northwestern China

Boreal winter (December–January–February, DJF) precipitation in northwestern China during the Holocene has been revealed to contribute a great deal to moisture evolution in northwestern China (Jin et al., 2012; Kutzbach et al., 2014; Wang and Feng, 2013). Figure 2 depicts the evolution of boreal winter rainfall in northwestern China (averaged rainfall over the region of 35°–50°N and 75°–100°E, black line) on orbital time scales (99-point filtered), showing a general increasing trend from 9 to 0 ka BP. This model result coincides with the synthesized moisture index from four proxy records in northwestern China (Figure 2, blue line) except a mismatch during the early Holocene. Proxy records revealed much drier climate in northwestern China during the early Holocene than the middle Holocene. However, the modelled DJF precipitation during the early Holocene resembled the middle Holocene, probably resulting from the neglecting of ice sheets and deglacial freshening of the North Atlantic in the HT simulation. The remnant LIS and meltwater into the North Atlantic could have weakened precipitation in northwestern China during the early Holocene (Jin et al., 2012), and their effects were negligible during the middle and late Holocene when the remnant LIS was disappearing by 7 ka BP (Peltier, 2004).

## Physical mechanisms responsible for Holocene changes in boreal winter rainfall over northwestern China

Orbitally driven insolation forcing is considered to be the most prominent forcing mechanism for Earth's long-term climate changes (Milankovitch, 1941). It is generally believed that variation of winter (DJF) precipitation in northwestern China is closely

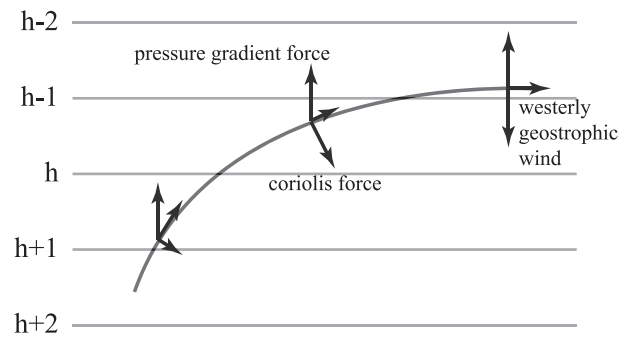


**Figure 1.** Schematic of the formation of the mid-latitude westerlies.  $h$  corresponds to geopotential heights.

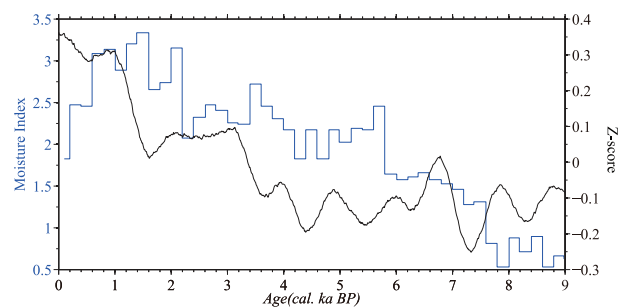


**Figure 2.** Comparison of simulated boreal winter (December–January–February, DJF) precipitation in northwestern China averaged over the region of 35°–50°N and 75°–100°E (black line, 99-point filtered) and synthesized moisture index from proxy records in northwestern China (blue line, Wang and Feng, 2013) during the Holocene.

linked to changes in the Northern Hemisphere westerly circulation during the Holocene (e.g. Chen et al., 2008; Jin et al., 2012; Wang and Feng, 2013). As shown in Figure 3a, mid-latitude winter westerly winds at 500 hPa upstream of northwestern China (35°–55°N, 0°–90°E) have shifted from weak to strong from the early to late Holocene, coinciding well with DJF rainfall in northwestern China (black line), with a correlation coefficient of 0.83 ( $p < 0.05$ ) on orbital time scales during the Holocene (9–0 ka BP). This significantly positive relationship between DJF rainfall in northwestern China and mid-latitude winter westerly winds is also seen in the middle and upper troposphere (Figure 4). However, it is in contrast to the result of Li et al. (2013), who found an inverse relationship between winter (DJF) precipitation in ACA and the westerly index on orbital time scales during the last 150 ka BP in a transient simulation. This is probably due to that the ‘westerly index’ defined in the study of Li et al. (2013) is different from ours, which was the global average of the sea level pressure (SLP) differences between 35°N and 55°N. This surface westerly index (Li et al., 2013) is similar to the AO index that is defined as the normalized difference in global zonal-averaged SLP anomalies between 35°N and 65°N (Li and Wang, 2003), which was suggested to be negatively correlated with boreal winter precipitation in ACA (Aizen et al., 2001; Huang et al., 2013).

The Coriolis effect is the key factor in the large-scale dynamics of the atmosphere driving prevailing westerlies at middle–high latitudes (Holton, 2004). Since DJF rainfall has a consistent significant positive relationship with westerlies throughout the middle to upper levels in the troposphere (Figure 4), we only use westerly winds at 500 hPa in the following analyses. The mean zonal winds over 35°–55°N and 0°–90°E at 500 hPa (Figure 3b, blue line) fit well with the westerly geostrophic wind (Figure 3b, black line), the latter is defined as the geopotential height gradient between 35°N and 55°N at 500 hPa over the area of 0°–90°E (Rossby et al., 1939), which is mainly controlled by temperature gradient ( $R = 0.94$ ,  $p < 0.05$ ) (Figure 3b, magenta line) that itself is

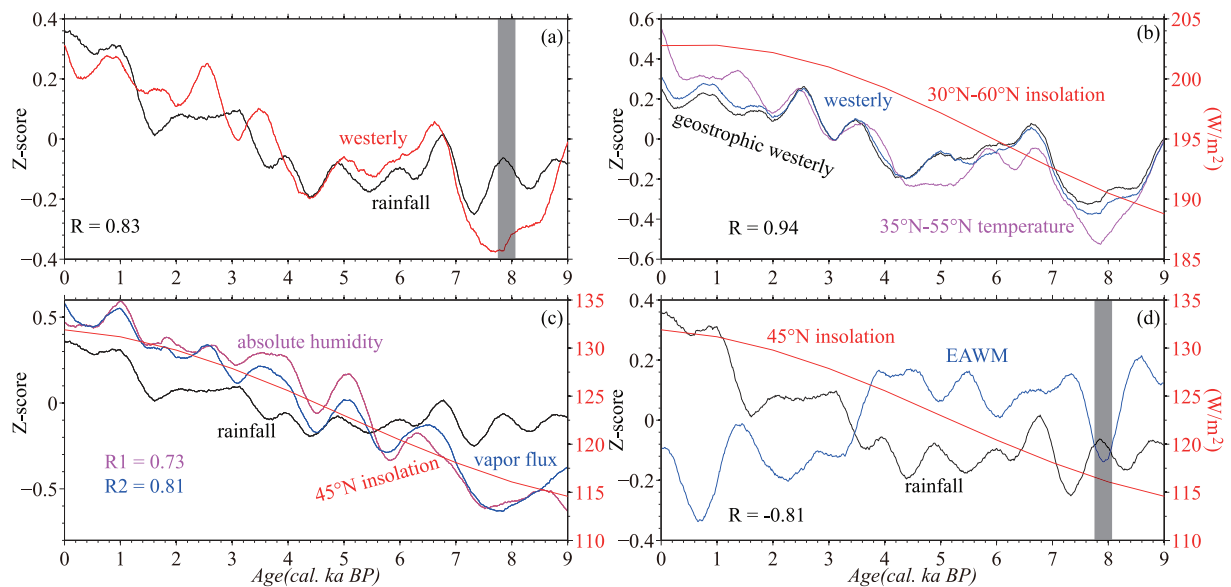


**Figure 3.** Holocene (9–0 ka BP) climate simulations as estimated by KCM HT experiment: (a) DJF precipitation in northwestern China averaged over the region of 35°–50°N and 75°–100°E (black line) and a comparison with DJF zonal mean winds (westerlies) averaged over 35°–55°N and 0°–90°E at 500 hPa (red line) on orbital time scales (99-point filtered); (b) Westerlies (blue line) and westerly geostrophic wind (black line) compared with the difference in tropospheric temperature between 35°N and 55°N at 500 hPa over the area of 0°–90°E (magenta line) on orbital time scales (99-point filtered). The difference in boreal winter (December) insolation between 30°N and 60°N (red line) is plotted for comparison. The westerly geostrophic wind is defined as the difference in geopotential height between 35°N and 55°N at 500 hPa over the area of 0°–90°E. (c) DJF precipitation in northwestern China (black line) compared with the absolute humidity (magenta line) and vapour flux (blue line) over the region of 35°–55°N and 0°–90°E at 500 hPa on orbital time scales (99-point filtered). December insolation at 45°N (red line) is plotted for comparison; (d) DJF precipitation in northwestern China (black line) compared with the strength of the EAWM (blue line) on orbital time scales (99-point filtered). December insolation at 45°N (red line) is plotted for comparison. The EAWM index is defined as the mean sea level pressure over the region of 40°–60°N and 70°–120°E (Gong et al., 2001).

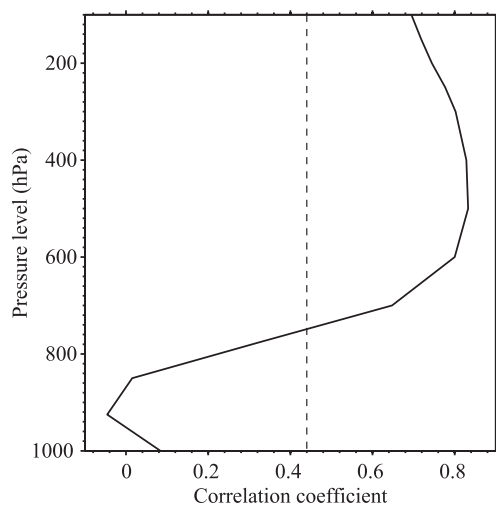


**Figure 4.** Correlation coefficients between DJF precipitation in northwestern China (35°–50°N and 75°–100°E) and westerlies at different geopotential heights. The dashed line is significant at the 95% significance level estimated with a Monte–Carlo experiment (Di Lorenzo et al., 2010; Livezey and Chen, 1983; Thompson, 1979).

dominated by the latitudinal insolation gradient (Figure 3b, red line). Accordingly, the westerly wind intensity is originally related to the insolation gradient. In other words, winter precipitation in northwestern China is closely related to the winter insolation gradient at mid-latitudes.

Resembling summer monsoonal winds that carry plenty of moisture from the Indian and Pacific oceans to the EASM region causing heavy rainfall during boreal summer, one important way that westerlies exert their influence on winter rainfall in northwestern China is via transporting moisture from North Atlantic

and Mediterranean, Black, Caspian Seas to northwestern China (Jin et al., 2012). The water vapour content (Figure 3c, magenta line) upstream of northwestern China experienced an increasing trend from the early to late Holocene. The upstream moisture content is closely related to winter precipitation in northwestern China, with a correlation coefficient of 0.73 ( $p < 0.05$ ) on orbital time scales during the Holocene (9–0 ka BP). The gradually increasing atmospheric moisture content follows the evolution of winter insolation at 45°N during the Holocene (9–0 ka BP) (Figure 3c, red line), which is because an enhanced winter insolation induced an increase in the evaporation over the North Atlantic, Mediterranean, Black and Caspian Seas. The strengthened westerly winds and the increased atmospheric moisture content can thus enhance moisture transport towards northwestern China (Figure 3c, blue line), which is significantly correlated with precipitation in this area ( $R = 0.81$ ,  $p < 0.05$ ). The atmospheric moisture over the North Atlantic, Mediterranean, Black and Caspian Seas can be transported to ACA via a wave train in the middle–upper troposphere (Figure 5a–c).

In addition to atmospheric moisture condition, the lower level atmospheric circulation (vertical movement) is an important factor for the formation of precipitation. During boreal winter, the lower level atmospheric circulation over Eurasia is dominated by the East Asian winter monsoon (EAWM) system with powerful Siberian High generating dry sinking airflow, which is unfavourable to the formation of precipitation in northwestern China. Simulated EAWM intensity was stronger during the early–middle Holocene (9–4 ka BP) and weaker during the late Holocene (4–0 ka BP) (Figure 3d, blue line), which is consistent with the proxy record revealed from aeolian sediments at the southern edge of the Gobi Desert, western China (Li and Morrill, 2014). The EAWM is negatively correlated with winter rainfall in northwestern China (Figure 3d), with a correlation coefficient of  $-0.81$  ( $p < 0.05$ ) on orbital time scales during the Holocene. Holocene evolution of the EAWM corresponds to the increasing winter



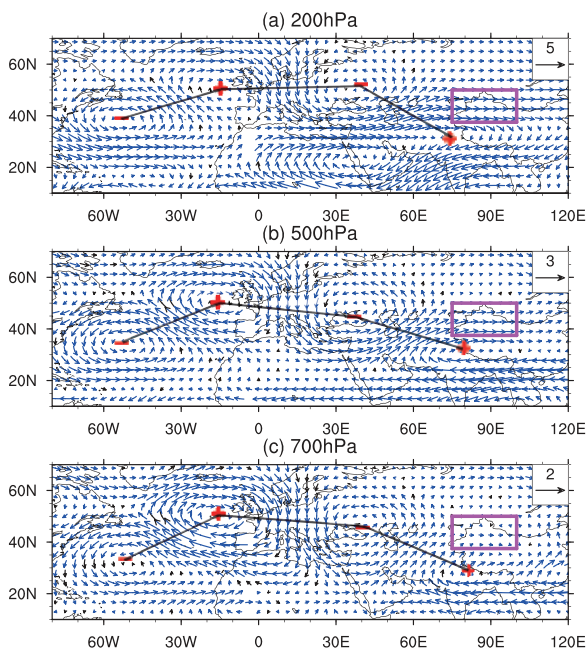


**Figure 5.** Composite differences in DJF mean wind fields (unit: m/s) at (a) 200hPa, (b) 500hPa and (c) 700hPa between the late (0.5–0 ka BP) and the early (9–8.5 ka BP) Holocene. Blue vectors indicate that differences are significant at the 95% significance level. The magenta box indicates the study area (35°–50°N and 75°–100°E) in northwestern China.

insolation (Figure 3d, red line). At ~8 ka BP, a relatively wet climate was accompanied by the weakest westerly intensity (Figure 3a, shading), which was probably related to the weak EAWM at that time (Figure 3d, shading).

In addition, cloud condensation nuclei (also known as cloud seeds) that serve as surfaces on which water vapour condenses are crucial to form rain. Tiny particles of dust can act as cloud condensation nuclei. ACA area, which is known as a main dust source of Asia, can provide sufficient cloud condensation nuclei to atmosphere to form rain. Moreover, the grain sizes of sediments in ACA area have shifted from coarse to fine from the early to late Holocene (An et al., 2011; Li and Morrill, 2014), suggesting more sufficient cloud condensation nuclei in the atmosphere during the late Holocene than that during the early Holocene.

## Conclusion

In this study, using simulation results from an atmosphere–ocean–sea-ice coupled general circulation model (KCM) forced by orbital variations, we analysed the physical mechanisms for orbital-scale evolution of winter rainfall in northwestern China during the period of 9–0 ka BP. Our simulations neglected other forcing factors, such as GHGs and ice sheets, which may misestimate the evolution of winter rainfall in northwestern China and hinder a full understanding of the associated physical mechanisms. However, these forcing factors are of minor importance compared with orbital forcing during the Holocene (Schneider et al., 2010), as also supported by the model–data comparison in this study (Figure 2).

Water vapour, vertical movement and condensation nucleus are critical to the formation of precipitation. In ACA, the condensation nucleus is not the limitation for precipitation since widely distributed deserts and sandy lands can provide sufficient condensation nucleus. The formation of winter rainfall in northwestern China is thus mainly determined by water vapour and vertical movement (dominated by the Siberian High). Hence, the responses of water vapour transportation and the EAWM to insolation forcing as well

as internal feedbacks of climate system are crucial to understand the physical mechanisms for winter precipitation in northwestern China during the Holocene.

Winter rainfall in northwestern China during the Holocene as estimated from the KCM simulation shows a persistently increasing trend, which is generally consistent with the moisture index evidenced by proxy records in northwestern China since ~8 ka BP (Wang and Feng, 2013). The continuously increasing winter precipitation in northwestern China during the Holocene is closely related to the mid-latitude westerly winds and the increase in vapour flux upstream this area. The westerly wind intensity is influenced by the insolation gradient at mid-latitudes that controls the meridional thermal difference. The water vapour content is closely related to insolation at mid-latitudes that affects surface temperature and thus the evaporation. In addition, winter rainfall in northwestern China is negatively related to the EAWM, which is also controlled by insolation at mid-latitude that regulates the surface temperature and thus the strength of the Siberian High during boreal winter season. Since Holocene evolution of the Asian summer monsoon is mainly controlled by summer insolation (e.g. Jin et al., 2014; Wang et al., 2005), we suggest that changes in the seasonal cycle of incoming solar radiation driven by Earth's orbital changes have probably played an important role in the out-of-phase relationship in the moisture evolution between the ACA and EASM regions during the Holocene.

## Acknowledgements

The modelling experiments using the KCM were performed at the Computer Centre of Kiel University, Germany. W Park and L Mojib of GEOMAR Helmholtz-Zentrum für Ozeanforschung Kiel and Birgit Schneider of Christian-Albrechts-Universität zu Kiel are thanked for their kind help and thoughtful discussion during the use of the KCM for the simulation experiments.

## Funding

This work was jointly supported by the National Natural Science Foundation of China (NSFC; 41275071), the State Key Programme of the NSFC (41130102), the National Basic Research Programme of China (973 Programme; 2012CB955301) and the Fundamental Research Funds for the Central Universities (Izujbky-2015-218).

## References

- Aizen EM, Aizen VB, Melack JM et al. (2001) Precipitation and atmospheric circulation patterns at mid-latitudes of Asia. *International Journal of Climatology* 21: 535–556.
- An CB, Lu YB, Zhao JJ et al. (2012) A high-resolution record of Holocene environmental and climatic changes from Lake Balikun (Xinjiang, China): Implications for central Asia. *The Holocene* 22: 43–52.
- An CB, Zhao J, Tao S et al. (2011) Dust variation recorded by lacustrine sediments from arid Central Asia since ~15 cal ka BP and its implication for atmospheric circulation. *Quaternary Research* 75: 566–573.
- Berger A and Loutre MF (1991) Insolation values for the climate of the last 10 million years. *Quaternary Science Reviews* 10: 297–317.
- Chen FH, Chen JH, Holmes J et al. (2010) Moisture changes over the last millennium in arid central Asia: A review, synthesis and comparison with monsoon region. *Quaternary Science Reviews* 29: 1055–1068.
- Chen FH, Huang W, Jin LY et al. (2011) Spatiotemporal precipitation variations in the arid Central Asia in the context of global warming. *Science in China Series D: Earth Sciences* 54: 1812–1821.
- Chen FH, Huang XZ, Zhang JW et al. (2006) Humid little ice age in and central Asia documented by Bosten Lake, Xinjiang,

- China. *Science in China Series D: Earth Sciences* 49: 1280–1290.
- Chen FH, Yu ZC, Yang ML et al. (2008) Holocene moisture evolution in arid central Asia and its out-of-phase relationship with Asian monsoon history. *Quaternary Science Reviews* 27: 351–364.
- Chen G and Huang R (2012) Excitation mechanisms of the teleconnection patterns affecting the July precipitation in Northwest China. *Journal of Climate* 25: 7834–7851.
- Chen JH, Chen FH, Feng S et al. (2015) Hydroclimatic changes in China and surroundings during the Medieval Climate Anomaly and Little Ice Age: Spatial patterns and possible mechanisms. *Quaternary Science Reviews* 107: 98–111.
- Dallmeyer A, Claussen M, Fischer N et al. (2015) The evolution of sub-monsoon systems in the Afro-Asian monsoon region during the Holocene – Comparison of different transient climate model simulations. *Climate of the Past* 10: 2293–2353.
- Dando WA (2005) *Asia: Climates of Siberia, central and east Asia*. In: Oliver JE (ed.) *Encyclopedia of World Climatology*. Dordrecht: Springer, pp. 102–114.
- Di Lorenzo E, Cobb KM, Furtado JC et al. (2010) Central Pacific El Niño and decadal climate change in the North Pacific. *Nature Geoscience* 3: 762–765.
- Ding Q and Wang B (2005) Circumglobal teleconnection in the Northern Hemisphere summer. *Journal of Climate* 18: 3483–3505.
- Ding Y, Sun Y, Wang Z et al. (2009) Inter-decadal variation of the summer precipitation in China and its association with decreasing Asian summer monsoon. Part II: Possible causes. *International Journal of Climatology* 28: 1926–1944.
- Ding Y, Wang Z and Sun Y (2008) Inter-decadal variation of the summer precipitation in East China and its association with decreasing Asian summer monsoon. Part I: Observed evidences. *International Journal of Climatology* 28: 1139–1161.
- Feng S, Nadarajah S and Hu Q (2007) Modeling annual extreme precipitation in China using generalized extreme value distribution. *Journal of the Meteorological Society of Japan* 85: 599–613.
- Gong D, Wang S and Zhu J (2001) East Asian winter monsoon and Arctic Oscillation. *Geophysical Research Letters* 28: 2073–2076.
- Haug GH, Hughen KA, Sigman DM et al. (2001) Southward migration of the intertropical convergence zone through the Holocene. *Science* 293: 1304–1308.
- Holton JR (2004) *An Introduction to Dynamic Meteorology*. New York: Academic Press.
- Huang G, Liu Y and Huang R (2011) The interannual variability of summer rainfall in the arid and semiarid regions of Northern China and its association with the northern hemisphere circumglobal teleconnection. *Advances in Atmospheric Sciences* 28: 257–268.
- Huang W, Chen FH, Feng S et al. (2013) Interannual precipitation variations in the mid-latitude Asia and their association with large scale atmospheric circulation. *Chinese Science Bulletin* 58: 3962–3968.
- Huang W, Chen JH, Zhang XJ et al. (2015a) Definition of the core zone of the ‘westerlies-dominated climatic regime’, and its controlling factors during the instrumental period. *Science China: Earth Science* 58: 676–684.
- Huang W, Feng S, Chen JH et al. (2015b) Physical mechanisms of summer precipitation variations in the Tarim Basin in Northwest China. *Journal of Climate* 28: 3579–3591.
- Huang XZ, Chen FH, Fan YX et al. (2009) Dry late-glacial and early Holocene climate in arid central Asia indicated by lithological and palynological evidence from Bosten Lake, China. *Quaternary International* 194: 19–27.
- Jiang FQ, Zhu C, Mu GJ et al. (2005) Magnification of flood disasters and its relation to regional precipitation and local human activities since the 1980s in Xinjiang, Northwestern China. *Natural Hazards* 36: 307–330.
- Jin L, Chen F, Morrill C et al. (2012) Causes of early Holocene desertification in arid central Asia. *Climate Dynamics* 38: 1577–1591.
- Jin L, Schneider B, Park W et al. (2014) The spatial-temporal patterns of Asian summer monsoon precipitation in response to Holocene insolation change: A model-data synthesis. *Quaternary Science Reviews* 85: 47–62.
- Kutzbach JE, Chen G, Cheng H et al. (2014) Potential role of winter rainfall in explaining increased moisture in the Mediterranean and Middle East during periods of maximum orbitally-forced insolation seasonality. *Climate Dynamics* 42: 1079–1095.
- Latif M, Park W, Ding H et al. (2009) Internal and external North Atlantic sector variability in the Kiel Climate Model. *Meteorologische Zeitschrift* 18: 433–443.
- Lee JY, Wang B, Seo KH et al. (2014) Future change of Northern Hemisphere summer tropical–extratropical teleconnection in CMIP5 models. *Journal of Climate* 27: 3643–3664.
- Leroy SAG, López-Merino L, Tudryn A et al. (2014) Late Pleistocene and Holocene palaeoenvironments in and around the middle Caspian basin as reconstructed from a deep-sea core. *Quaternary Science Reviews* 101: 91–110.
- Levitus S (1982) *Climatological atlas of the world ocean*. NOAA professional paper 13, December. Washington: NOAA/ERL GFDL, p. 173.
- Li JP and Wang JXL (2003) A modified zonal index and its physical sense. *Geophysical Research Letters* 30(12): 1632.
- Li X, Liu X, Qiu L et al. (2013) Transient simulation of orbital-scale precipitation variation in monsoonal East Asia and arid central Asia during the last 150ka. *Journal of Geophysical Research: Atmospheres* 118: 7481–7488.
- Li Y and Morrill C (2014) A Holocene East Asian winter monsoon record at the southern edge of the Gobi Desert and its comparison with a transient simulation. *Climate Dynamics*. Epub ahead of print 21 October. DOI: 10.1007/s00382-014-2372-5.
- Livezey RE and Chen WY (1983) Statistical field significance and its determination by Monte Carlo techniques. *Monthly Weather Review* 111: 46–59.
- Long H, Shen J, Tsukamoto S et al. (2014) Dry early Holocene revealed by sand dune accumulation chronology in Bayanbulak Basin (Xinjiang, NW China). *The Holocene*. Epub ahead of print 5 March. DOI: 10.1177/0959683614523804.
- Lorenz S and Lohmann G (2004) Acceleration technique for Milankovitch type forcing in a coupled atmosphere-ocean circulation model: Method and application for the Holocene. *Climate Dynamics* 23: 727–743.
- Madec G (2008) NEMO ocean engine. Note du Pole de modélisation, Institut Pierre-Simon Laplace (IPSL), France, No 27. Available at: <http://nora.nerc.ac.uk/id/eprint/164324>.
- Milankovitch MM (1941) *Canon of Insolation and the Ice-Age Problem*. Beograd: Koniglich Serbische Akademie [English translation by the Israel Program for Scientific Translations. Washington, DC: US Department of Commerce, and National Science Foundation].
- Park W and Latif M (2008) Multidecadal and multicentennial variability of the meridional overturning circulation. *Geophysical Research Letters* 35: L22703.
- Park W and Latif M (2010) Pacific and Atlantic multidecadal variability in the Kiel Climate Model. *Geophysical Research Letters* 37: L24702.
- Park W, Keenlyside N, Latif M et al. (2009) Tropical Pacific climate and its response to global warming in the Kiel Climate Model. *Journal of Climate* 22: 71–92.

- Peltier WR (2004) Global glacial isostasy and the surface of the ice-age earth: The ICE-5G (VM2) model and GRACE. *Annual Review of Earth and Planetary Sciences* 32: 111–149.
- Roeckner E, Bauml G, Bonaventura L et al. (2003) *The atmospheric general circulation model ECHAM5. Part I: Model description*. Max Planck Institute for Meteorology, Report no. 349, November. Hamburg: Max Planck Institute for Meteorology, 127 pp.
- Rossby CG and Collaborators (1939) Relation between variations in the intensity of the zonal circulation of the atmosphere and the displacements of the semi-permanent centers of action. *Journal of Marine Research* 2: 38–55.
- Schneider B, Leduc G and Park W (2010) Disentangling seasonal signals in Holocene climate trends by satellite-model-proxy integration. *Paleoceanography* 25: PA4217.
- Shi YF, Shen YP, Kang E et al. (2007) Recent and future climate change in Northwest China. *Climatic Change* 80: 379–393.
- Su MF and Wang HJ (2007) Relationship and its instability of ENSO–Chinese variations in droughts and wet spells. *Science in China Series D: Earth Sciences* 50: 145–152.
- Thompson RORY (1979) Coherence significance levels. *Journal of the Atmospheric Sciences* 36: 2020–2021.
- Valcke S (2006) *OASIS3 user guide (prism\_2–5)*. PRISM support initiative, Report no. 3, 68 pp. Available at: [http://www.prism.enes.org/Publications/Reports/oasis3\\_UserGuide\\_T3.pdf](http://www.prism.enes.org/Publications/Reports/oasis3_UserGuide_T3.pdf).
- Wang W and Feng Z (2013) Holocene moisture evolution across the Mongolian Plateau and its surrounding areas: A synthesis of climatic records. *Earth-Science Reviews* 122: 38–57.
- Wang YJ, Cheng H, Edwards RL et al. (2005) The Holocene Asian Monsoon: Links to solar changes and North Atlantic Climate. *Science* 308: 854–857.
- Xu C, Li J, Zhao J et al. (2015) Climate variations in northern Xinjiang of China over the past 50 years under global warming. *Quaternary International* 358: 83–92.
- Yang J, Liu Q, Xie S-P et al. (2007) Impact of the Indian Ocean SST basin mode on the Asian summer monsoon. *Geophysical Research Letters* 34: L02708.
- Ye H and Lu R (2012) Dominant patterns of summer rainfall anomalies in east China during 1951–2006. *Advances in Atmospheric Sciences* 29: 695–704.
- Zhang X, Jin L and Jia W (2015) Centennial-scale teleconnection between North Atlantic sea surface temperatures and the Indian summer monsoon during the Holocene. *Climate Dynamics*. Epub ahead of print 29 July. DOI: 10.1007/s00382-015-2771-2.